




Developmental effects of two different copper oxide nanomaterials in sea urchin (*Lytechinus pictus*) embryos

Cristina Torres-Duarte, Adeyemi S. Adeleye, Suman Pokhrel, Lutz Mädler, Arturo A. Keller & Gary N. Cherr


To cite this article: Cristina Torres-Duarte, Adeyemi S. Adeleye, Suman Pokhrel, Lutz Mädler, Arturo A. Keller & Gary N. Cherr (2016) Developmental effects of two different copper oxide nanomaterials in sea urchin (*Lytechinus pictus*) embryos, *Nanotoxicology*, 10:6, 671-679, DOI: [10.3109/17435390.2015.1107145](https://doi.org/10.3109/17435390.2015.1107145)


To link to this article: <http://dx.doi.org/10.3109/17435390.2015.1107145>

 View supplementary material [↗](#)

 Published online: 08 Dec 2015.

 Submit your article to this journal [↗](#)

 Article views: 152

 View related articles [↗](#)

 View Crossmark data [↗](#)

 Citing articles: 1 View citing articles [↗](#)

ORIGINAL ARTICLE

Developmental effects of two different copper oxide nanomaterials in sea urchin (*Lytechinus pictus*) embryos

Cristina Torres-Duarte¹, Adeyemi S. Adeleye², Suman Pokhrel³, Lutz Mädler³, Arturo A. Keller², and Gary N. Cherr^{1,4}

¹Bodega Marine Laboratory, University of California, Davis, Bodega Bay, CA, USA, ²Bren School of Environmental Science & Management, University of California, Santa Barbara, CA, USA, ³Foundation Institute of Materials Science (IWT), Department of Production Engineering, University of Bremen, Bremen, Germany, and ⁴Department of Environmental Toxicology and Nutrition, University of California, Davis, CA, USA

Abstract

Copper oxide nanomaterials (nano-CuOs) are widely used and can be inadvertently introduced into estuarine and marine environments. We analyzed the effects of different nano-CuOs (a synthesized and a less-pure commercial form), as well as ionic copper (CuSO₄) on embryo development in the white sea urchin, a well-known marine model. After 96 h of development with both nano-CuO exposures, we did not detect significant oxidative damage to proteins but did detect decreases in total antioxidant capacity. We show that the physicochemical characteristics of the two nano-CuOs play an essential role in their toxicities. Both nano-CuOs were internalized by embryos and their differential dissolution was the most important toxicological parameter. The synthesized nano-CuO showed greater toxicity (EC₅₀ = 450 ppb of copper) and had increased dissolution (2.5% by weight over 96 h) as compared with the less-pure commercial nano-CuO (EC₅₀ = 5395 ppb of copper, 0.73% dissolution by weight over 96 h). Copper caused specific developmental abnormalities in sea urchin embryos including disruption of the aboral-oral axis as a result in changes to the redox environment caused by dissolution of internalized nano-CuO. Abnormal skeleton formation also occurred.

Keywords

Embryonic axis disruption, nanoparticle dissolution, oxidative stress, sea urchin embryo development

History

Received 28 May 2015
Revised 31 August 2015
Accepted 20 September 2015
Published online 4 December 2015

Introduction

Nanomaterials (NMs) are highly heterogeneous, and even if they have the same chemical composition, the individual NMs can have different physicochemical properties (e.g. size, shapes, surface areas and optical properties), affecting their bioavailability and toxicity (Nel et al., 2009). Moreover, properties of the media in which NMs are dispersed such as pH, dissolved organic matter and ionic strength play important roles in NM aggregation, sedimentation, dissolution and bioavailability/toxicity (Adeleye et al., 2014; Conway et al., 2015; Keller et al., 2010; Nel et al., 2009; Oberdorster, 2010; Shi et al., 2011).

The toxicity of metallic NMs can be caused either by the dissolved ions, the particles or both. Some studies attribute the toxic effects solely to the ions released into the media (Cho et al., 2012; Fairbairn et al., 2011; Gunawan et al., 2011; Xia et al., 2008), while others have demonstrated that NMs are more toxic than their bulk counterparts (Amorim & Scott-Fordsmand, 2012; Bielmyer-Fraser et al., 2014; Garner et al., 2015; George et al., 2012; Shi et al., 2011; Siddiqui et al., 2015; Thit et al., 2013). For example, hatching inhibition in zebrafish embryos is caused by metal oxide NM dissolution and this effect is similar to ionic forms of the metals (Lin et al., 2013; Lin et al., 2011; Xia et al., 2011), while an NM-specific effect was observed in earthworms exposed to nano-Cu (Amorim & Scott-Fordsmand, 2012). Therefore, understanding the fate, transport and transformations

of NMs in different media and in different organisms during different life stages is critical to understanding their impacts in different ecosystems.

The release of ions from metallic NMs can be a desirable feature in certain applications. For example, copper NMs and its oxides are used as an alternative additive in antifouling paints since in a nano-particulate form, copper dissolution can be very slow, releasing ions into the environment over extended periods of time (Cao et al., 2011). Some of these NMs may be released from antifouling paint matrices into the aquatic environment, where they can exert their toxic effects in non-target organisms (Rawat et al., 2010). Previous toxicological studies of copper oxide nanomaterial (nano-CuO) in marine and estuarine organisms show that the NMs can accumulate in the tissue and cause oxidative stress, inhibit enzymatic activity, affect embryonic development and defense mechanisms at low concentrations, and at high doses, can cause mortality (Gomes et al., 2011; Hanna et al., 2014; Hanna et al., 2013; Hu et al., 2014; Wu et al., 2015). We selected the sea urchin as our model system for studying the potential impact of nano-CuO in coastal environments, focusing on the most sensitive developmental stages (Hamdoun & Epel, 2007). Exposure to chemicals during early development has major impacts on the establishment of the embryonic axis of sea urchins, affecting their morphology, development and survival as larvae (Fernández & Beiras, 2001; Pillai et al., 2003). Though toxicity of nano-CuO in sea urchin embryos has been previously studied (Wu et al., 2015), detailed studies on the mechanisms of nano-CuO developmental toxicity are lacking. In the present study, we investigated the effects of soluble Cu²⁺ and two nano-CuOs on sea urchin embryo development. We used a commercial

nano-CuO as well as an in-house FSP synthesized nano-CuO that has a higher purity and dissolution rate, in order to investigate the influence of physicochemical characteristics of nano-CuO on development, copper uptake and oxidative stress.

Materials and methods

Nanomaterials source and characterization

Commercial nano-CuO was obtained from Sigma–Aldrich (St. Louis, MO), and has been previously characterized (Adeleye et al., 2014). Their major physicochemical properties are summarized in Table 1. The in-house synthesized nano-CuO (further referred as “synthesized nano-CuO”) was prepared using flame spray pyrolysis (FSP) as described earlier (Pokhrel et al., 2012; Teoh et al., 2010), and was characterized using X-ray diffraction (XRD), transmission electron microscopy (TEM) and Brunauer–Emmett–Teller (BET) measurements (Pokhrel et al., 2009). Methodology details for both synthesis and characterization are provided in the Supplementary Material. The size and surface charge of synthesized nano-CuO were determined measuring hydrodynamic size and zeta potential as described earlier using a Malvern Zetasizer Nano-ZS90 (Worcestershire, UK) (Adeleye et al., 2014; Adeleye & Keller, 2014). The isoelectric point was determined titrating the suspension of NMs with dilute HCl and NaOH (Fisher Scientific, Fair Lawn, NJ). Size and morphology of both pristine nano-CuO were investigated via scanning electron microscopy (SEM, FEI XL40 Sirion (Hillsboro, OR), equipped with an Oxford INCA probe for energy-dispersive X-ray spectroscopy (Oxfordshire, UK)) and TEM.

Stability in 0.45- μ m filtered seawater (FSW; collected from the Pacific Ocean at Bodega Bay, CA) of both nano-CuO was characterized with aggregation and sedimentation kinetics studies via dynamic light scattering (Malvern Zetasizer, Worcestershire, UK) and spectrophotometry ($\lambda = 390$ nm; Shimadzu 1601 UV-Vis spectrophotometer Kyoto, Japan), respectively (Adeleye et al., 2014; Conway et al., 2015). Stocks of both nano-CuO were diluted in either de-ionized water (DI; 18.2 M Ω .cm, Barnstead Nanopure Diamond; Thermo Scientific, Waltham, MA) or FSW to achieve 50 ppm, and mixed thoroughly (5 s; Misonix Sonicator S-4000, QSonica LLC, Newtown, CT) before measurements.

Nanomaterial dispersion

Stock dispersions of 1000 ppm of both nano-CuO were prepared as previously reported (Fairbairn et al., 2011; Wu et al., 2015), and details are provided in the Supplemental Material. A range of nano-CuO suspensions were prepared in 0.45 μ m FSW containing 0.2 ppm of alginic acid (Sigma–Aldrich, St. Louis, MO) and stored for 96 h at 16 °C. Alginic acid is produced by brown algae and is a source of organic carbon and was used in concentrations similar to what can be found in natural marine environments; this

also helps increase nanoparticle stability in the water column (Loosli et al., 2013). NMs were separated from soluble copper by centrifugation at 14 000 $\times g$ for 10 min in an Eppendorf Microcentrifuge 5417C (Thermo Scientific, Waltham, MA) using Amicon Ultra-0.5 Ultracel 3 centrifuge tubes (3 kDa cutoff, Millipore, Billerica, MA). The filtrate was acidified to pH 1.7 with trace metal grade HCl (Fisher Scientific, Fair Lawn, NJ) 6N and stored until analysis. Total copper concentration was also determined using chemiluminescence (Durand et al., 2013; Wu et al., 2015), which has a linear response ($R^2 = 0.9942$) from 1 to 70 ppb copper (Supplementary Material).

Sea urchin embryo culture and development

Adult white sea urchins (*Lytechinus pictus*) were maintained at the University of California Davis Bodega Marine Laboratory (Bodega Bay, CA) in flow-through seawater tanks. Gametes were collected and fertilized as described previously (Fairbairn et al., 2011; Wu et al., 2015). Fertilization success was assessed under the microscope and only batches of embryos exhibiting >90% successful fertilization were used for exposure to 5–100 ppb of copper from copper sulfate (CuSO₄, Sigma–Aldrich, St. Louis, MO), 20–2000 ppb of copper from commercial nano-CuO and 380–38 000 ppb of copper from synthesized nano-CuO dispersed in 0.45 μ m FSW containing a final concentration of 0.2 ppm alginic acid. CuSO₄ solutions were prepared the same way as the nano-CuOs dispersions (Supplementary Material). Embryos were exposed in 12-well polystyrene culture plates (5 mL/well, 100 embryos/mL) at 16 °C from 1 h after fertilization until controls (cultured in 0.2 ppm alginic acid in 0.45 μ m FSW) reached the pluteus larval stage (~96 h after fertilization). Samples were fixed with a final concentration of 0.1% paraformaldehyde (Electron Microscopy Sciences, Hatfield, PA) in FSW and for each replicate, 100 embryos were assessed for normal development using a Nikon AZ100 macrozoom stereo microscope (Melville, NY) at 40 \times magnification. Embryos were considered abnormal if skeletal-radialized plutei (abnormal skeletal rod angle), asymmetric internal skeleton, inhibited or delayed development or bell-like morphology (“oralized”) were observed (Figure 4). Experiments were reproduced at least 3 times, and for each experiment, treatments were always conducted in triplicate. To analyze skeleton formation, embryos were imaged with an Olympus BH-2 microscope (Tokyo, Japan) equipped with a polarized light attachment at 20 \times magnification.

For biochemical assays, the same conditions for embryo exposure were replicated in 500 mL polymethylpentene containers containing 200 mL of the corresponding treatment. After 96-h exposure, embryos were collected and total biomass (wet weight) was determined gravimetrically. Approximately 20% of the embryos were used for tissue copper quantification; the remainder was used for protein extraction by homogenization of the tissue

Table 1. Major physicochemical properties of synthesized and commercial nano-CuO particles used in this study.

Property	Synthesized nano-CuO	Commercial nano-CuO
Primary size (nm)	$d_{\text{XRD}} = 8.7$ $d_{\text{BET}} = 11.7$ $d_{\text{TEM}} = 10$	50 ^a
Particle size in DI water at pH 7 (nm)	205 \pm 11	280 \pm 15
Phase	Monoclinic	Monoclinic
Zeta potential in FSW (mV)	–1.15	–2.81
Isoelectric point	6.8	6.3
Surface area (m ² /g)	78.5	12.3
Purity (wt. %)	99	93
Dissolution in FSW (%)	2.5 ^b	0.74 ^c

^aAs reported by the manufacturer.

^b2000 ppb.

^c1900 ppb initial concentration.

using a probe sonicator (Microson Ultrasonic Cell Disruptor, Heat Systems) in HEPES (Sigma–Aldrich, St. Louis, MO) buffer (50 mM, pH 7.4) containing protease inhibitor cocktail (Sigma–Aldrich, St. Louis, MO). Samples were centrifuged at $14\,000 \times g$ for 10 min to eliminate tissue residues. Supernatant was used for further analyses.

Total antioxidant capacity

The total antioxidant capacity (TAOC) was determined using a modified version of the method of Miller & Rice-Evans (1997). Briefly, samples were mixed with a solution containing $5\ \mu\text{M}$ myoglobin (Sigma–Aldrich, St. Louis, MO), $140\ \mu\text{M}$ ABTS (Sigma–Aldrich, St. Louis, MO) and $180\ \mu\text{M}$ hydrogen peroxide (Sigma–Aldrich, St. Louis, MO) in potassium phosphate (Sigma–Aldrich, St. Louis, MO) buffer (5 mM, pH 7.4) supplemented with 0.9% NaCl (Sigma–Aldrich, St. Louis, MO) and 0.1% glucose (Sigma–Aldrich, St. Louis, MO). Absorbance of $\text{ABTS}^{\bullet+}$ at 400 nm was measured in duplicates in each plate in a TECAN GENios microplate reader (Maennedorf, Switzerland). The absorbance in the sample was compared with a standard curve of the antioxidant compound Trolox (Cayman Chemical, Ann Arbor, MI). Results were normalized to protein concentration that was determined by the method of Bradford (1976), using bovine serum albumin ($5\text{--}50\ \mu\text{g}/\text{mL}$) as a standard.

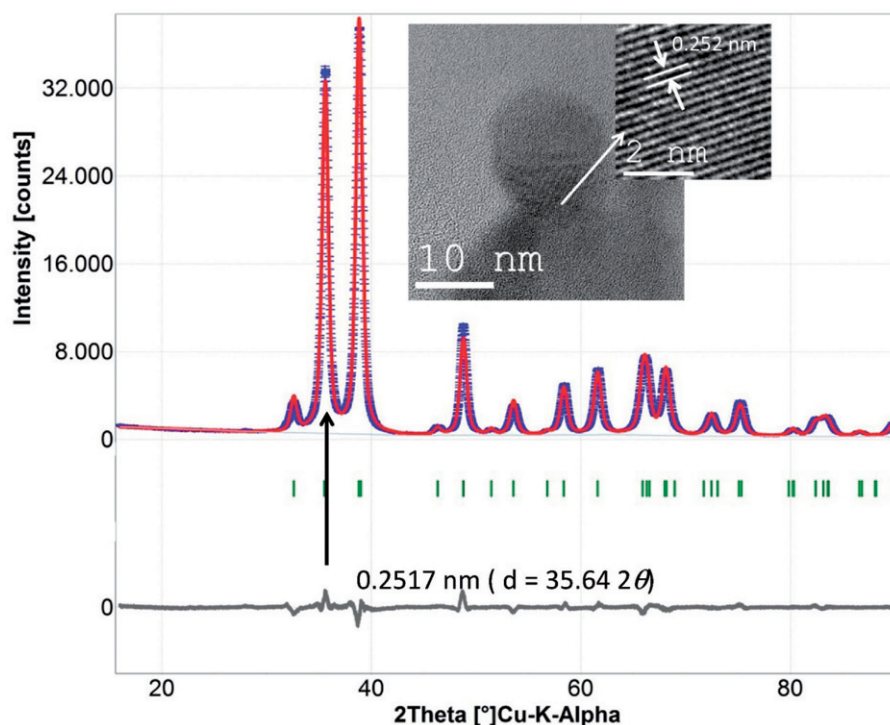
Tissue copper content and copper measurement

To determine the tissue copper concentration after exposure, embryos were treated as previously reported (Wu et al., 2015). The copper concentration in seawater (total and dissolved) and tissue, was determined using chemiluminescence, as described in the Supplementary Material.

Statistical analysis

The data obtained were tested using one-way analysis of variance (ANOVA) or the Kruskal–Wallis one-way ANOVA on Ranks. If significant, pairwise multiple comparison procedures were conducted, using the Tukey test or the Dunn's method.

Figure 1. X-ray diffraction patterns of FSP synthesized nano-CuO and matching the lattice spacing with the diffraction angles. Results show that most of the NMs are found to orient toward [0 0 2] direction.



Statistical significance was set at $p < 0.05$. Analyses were performed using SigmaPlot 11.0 (Erkrath, Germany).

Results

Nanomaterial characterization

A typical Rietveld-refined XRD pattern of the synthesized nano-CuO is presented in Figure 1. The cell parameters are: $a = 4.6869$, $b = 3.42154\ \text{\AA}$, $c = 3.1297\ \text{\AA}$, $\beta = 99.53^\circ$. The lattice parameters determined are close to the reported values (Åsbrink & Waśkowska, 1991). The d -spacing of $0.252\ (\pm 0.008)$ nm determined from high-resolution TEM (HRTEM) agreed reasonably with $d_{002} = 0.2517\ \text{nm}$ occurring at $35.64^\circ\ 2\theta$ for CuO (from XRD). The large specific surface area of synthesized nano-CuO [$78.5\ (\pm 3)\ \text{m}^2/\text{g}$] obtained by FSP suggested ultrafine particles with $11.7\ \text{nm}$ size similar to the crystallite size of 8.7 , obtained using Reitveld refinement. The morphology of the NMs was studied using low- and high-resolution TEM. Representative TEM images are presented in Figure 1 and magnified lattice arrangement is shown in the inset. The sizes of the particles were measured on an ensemble of 50 particles along and perpendicular to their axes. The average diameter of a single particle was found to be $\sim 10\ \text{nm}$.

SEM images of synthesized and commercial nano-CuO are presented in Supplementary Figure S1. Similar to the primary particle size, the initial hydrodynamic diameter (Adeleye et al., 2014) of commercial nano-CuO was greater than that of synthesized nano-CuO in DI water at pH 7 (Table 1).

Nanomaterial behavior in aqueous media

Nanomaterials' behavior in aqueous media is typically characterized in DI water, in which they are often very stable. However, the behavior in this ideal condition can be significantly different from a more environmentally relevant media such as FSW. To facilitate comparison with other published data, nanoparticles were characterized in both media. In addition, release of NMs into marine systems, at times, occurs via an intermediate freshwater system (e.g. river and wastewater). Hence, it is important to characterize nanoparticles in both media in order to properly

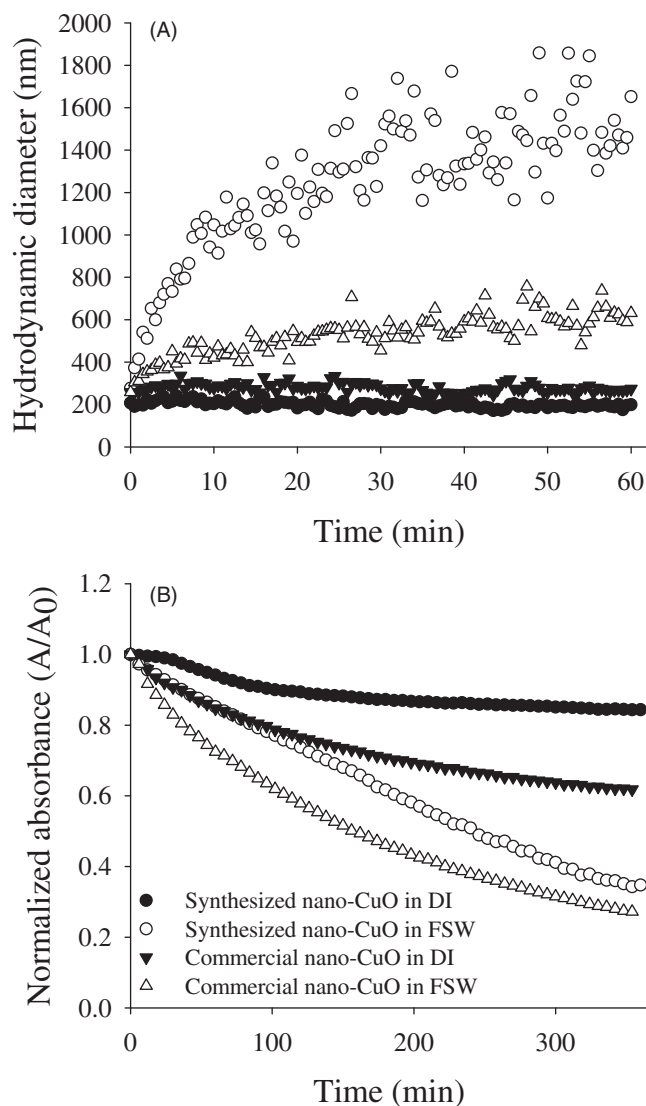


Figure 2. (A) Aggregation and (B) sedimentation rates of nano-CuO in DI and FSW. Synthesized nano-CuO forms larger aggregates but has a lower sedimentation rate than commercial nano-CuO in FSW.

predict their fate and effects in both media. Both nano-CuOs were relatively stable in DI water as indicated by hydrodynamic size measurements (Figure 2A). In FSW, however, the hydrodynamic diameter of both nanoparticles doubled within 1 h. The aggregation rate of synthesized nano-CuO in FSW was much higher than that of commercial nano-CuO (Figure 2A). However, despite having aggregates in an average 42% smaller, commercial nano-CuO sedimented faster than synthesized nano-CuO in both DI and FSW (Figure 2B).

The nano-CuOs used in this study had differing purity (Table 1), and thus different copper concentrations based on mass. Synthesized nano-CuO had 79% w/w of copper while commercial nano-CuO had 74% w/w. To facilitate comparisons, concentrations are expressed based on nominal total copper concentration for the corresponding treatment. The dissolution of NMs in FSW was analyzed after 96 h. Synthesized nano-CuO released 17 ppb of copper from a 200 ppb dispersion (8.5%), and 50 ppb of copper from a 2000 ppb dispersion (2.5%). Commercial nano-CuO showed lower dissolution, releasing 14 ppb of copper from a 1900 ppb dispersion (0.74%) and 31 ppb of copper from a 19 000 ppb dispersion (0.16%).

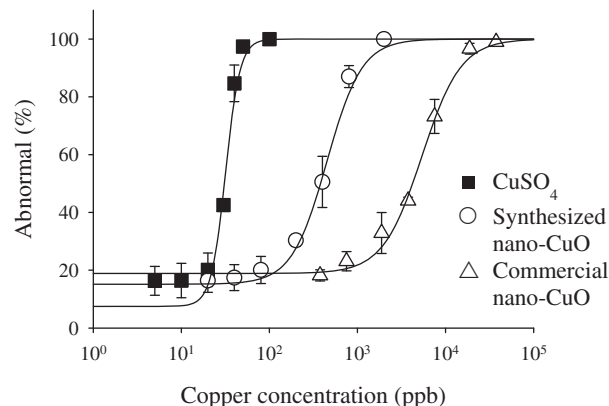


Figure 3. Dose–response curve for CuSO₄ (EC₅₀=32 ppb copper); synthesized nano-CuO (EC₅₀=450 ppb copper) and commercial nano-CuO (EC₅₀=5395 ppb copper) on development of *Lytechinus pictus* embryos after 96-h exposure.

Toxicity and developmental effects in sea urchin embryos exposed to soluble copper and nano-CuO

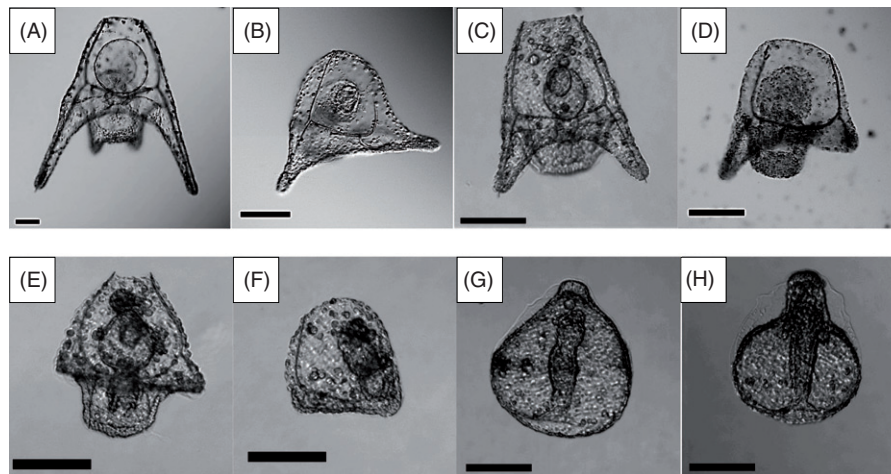
The toxicity varied depending on the source of copper (Figure 3). CuSO₄ was the most toxic (EC₅₀=32 ppb) followed by synthesized nano-CuO (EC₅₀=450 ppb), while commercial nano-CuO was the least toxic (EC₅₀=5395 ppb).

Copper caused diverse developmental effects in embryos. At low concentrations (<20 ppb CuSO₄, 200 ppb synthesized nano-CuO or 1800 ppb commercial nano-CuO), radialized plutei larvae were observed (<5%, Figure 4B), and ~20% of embryos were underdeveloped, observed as shorter arms and smaller size compared with control embryos (Figure 4A and C). At intermediate concentrations (20 ppb < CuSO₄ < 40 ppb; 200 ppb < synthesized nano-CuO < 700 ppb; 1800 ppb < commercial nano-CuO < 9300 ppb), effects on skeletal rod development were observed as asymmetric development and shorter postoral arms (Figure 4D). At low and intermediate concentrations of CuSO₄ and both nano-CuOs, there were no statistically significant differences in the the proportion of embryos presenting similar morphological effects. At high concentrations (>40 ppb CuSO₄, 700 ppb synthesized nano-CuO or 9300 ppb commercial nano-CuO), abnormal development of the skeleton and gut were observed (Figure 4E and F), with the most common effect being the formation of a cone-like constriction of the animal pole ectoderm resulting in a bell-like morphology (Hardin et al., 1992). This effect was statistically more significant at high concentrations of both nano-CuO particles (50% of embryos), compared with high concentrations of CuSO₄ (30% of embryos).

Effects on skeletal rod (spicule) development were observed under polarized light. At low and intermediate concentrations, the spicules were under-developed (Figure 5B), especially the postoral arms (Figure 5C). In ~10% of the embryos with bell-like morphology, more than two nucleation points of skeletal development (triradiate spicules) formed (Figure 5D and E), an effect previously reported in embryos exposed to other divalent cationic metals (Hardin et al., 1992), while in ~50% of the embryos no spicules formed (Figure 5F).

For subsequent experiments, 25 ppb of CuSO₄, 200 ppb of synthesized nano-CuO and 1900 ppb of commercial nano-CuO were selected as low-concentration exposures, where 35–40% of the embryos showed abnormal development. Approximately 50 ppb CuSO₄, 2000 ppb of synthesized nano-CuO and 19 000 ppb of commercial nano-CuO were considered as high concentrations where 100% of the embryos were abnormal. The percentages for each morphological effect observed in each treatment are listed in Supplementary Table S1.

Figure 4. Developmental effects in *Lytechinus pictus* embryos after 96 h of exposure to different sources of copper. (A) Normal development. (B) Radialized plutei. (C) Delayed skeletal development. (D) Asymmetric skeletal development. (E) Abnormal post-oral arm development. (F) Severe delayed skeletal development. (G) Bell-like malformation. (H) Severe bell-like malformation. Bar = 100 μ m.



Tissue copper accumulation and TAOC

Embryos exposed to 25 ppb of CuSO_4 accumulated the same amount of copper as embryos exposed to 200 ppb of synthesized nano-CuO (1.8 ng of copper/mg wet weight). There were no statistically significant differences in the amount of copper accumulated in embryos exposed to 50 ppb of CuSO_4 , 2000 ppb of synthesized nano-CuO, and 1900 ppb and 19 000 ppb of commercial nano-CuO (5.3 ± 1.1 , 7.9 ± 0.8 , 6.3 ± 1.5 and 11.9 ± 3.4 ng of copper/mg wet weight, respectively, Figure 6A).

Although protein oxidation has been used as an oxidative stress indicator (Shacter, 2000), and has been reported in mussels (Hu et al., 2014) and in sea urchin embryos (Wu et al., 2015) exposed to nano-CuO, we did not observe such protein oxidation in any of the treatments (Supplementary Figure S2). In contrast, there was a significant decrease in TAOC in embryos exposed to 2000 ppb of synthesized nano-CuO ($74 \pm 1.9\%$ of control), and was even lower in embryos exposed to 19 000 ppb of commercial nano-CuO ($57 \pm 2.1\%$ of control, Figure 6B).

Discussion

The behavior of NMs is highly dependent on the media where they are dispersed (Keller et al., 2010). Both nano-CuOs used in this study formed relatively stable aggregates in low ionic strength media. As expected, however, rapid aggregation was observed in FSW due to screening of electrostatic charge by FSW ions (Adeleye et al., 2014; Adeleye et al., 2013; Conway et al., 2015; Keller et al., 2010). Surface charge measurements confirmed this (charge screening), as the zeta potential of synthesized and commercial nano-CuO increased from -27.2 mV in DI to -1.15 mV in FSW and -34.4 mV in DI to -2.81 mV in FSW, respectively. The aggregation in FSW led to rapid sedimentation, with $>60\%$ of the initial particles settling out within 6 h. This suggests that benthic organisms such as sea urchins will be significantly exposed to these NMs if released into marine systems.

Copper is highly toxic for sea urchin embryos (King & Riddle, 2001; Kobayashi & Okamura, 2004; Rosen et al., 2008). In *Lytechinus pictus* embryos, we obtained an EC_{50} of 32 ppb of copper for CuSO_4 , which is similar to the value reported for *Paracentrotus lividus* (67 ppb of copper, Fernández & Beiras, 2001). The NMs used in this study were less toxic compared with the fully soluble CuSO_4 salt. However, synthesized nano-CuO was one order of magnitude more toxic than the commercial nano-CuO. This can be due to differences in their physicochemical properties (surface area, zeta potential, purity, size and dissolution, Table 1). Aggregates of nano-CuO in FSW can be

internalized by embryos during early development (Wu et al., 2015, Supplementary Figure S5), a period when embryos undergo very high levels of endocytosis (Covian-Nares et al., 2008), leading to higher intracellular concentrations of copper. The higher surface area of synthesized nano-CuO increases the contact points with the intracellular environment, and in combination with a higher zeta potential, can cause more cellular damage than commercial nano-CuO (Cho et al., 2012; Nel et al., 2009).

The toxicity of metal oxide NMs mediated by oxidative stress responses has been related to the metal oxide band gap (Zhang et al., 2012). However, nano-CuO does not seem to follow this rule, since it is highly toxic to mammalian cells, even though its band gap was outside the critical range of oxidation. Toxicity was attributed to its high dissolution (Zhang et al., 2012). Here, we have demonstrated that synthesized nano-CuO has a higher solubility than commercial nano-CuO (2.5% versus 0.74%, Table 1), probably due to differences in size and purity. The size of synthesized nano-CuO is ~ 10 nm while commercial nano-CuO is between 30 and 100 nm (Table 1 and Figure S1), and it has been demonstrated that small nanoparticles have higher dissolution rates than large particles (Midander et al., 2009). On the other hand, the presence of impurities in the commercial nano-CuO may lower its dissolution rate in a similar way as iron doping decreases the solubility of zinc oxide nanoparticles (nano-ZnO) and leads to a lower toxicity than non-doped nano-ZnO (George et al., 2011; Xia et al., 2011). Regardless, the amount of copper solubilized in FSW is not enough to explain the differences in NM toxicity, similarly to what has been reported in other marine organisms (Bielmyer-Fraser et al., 2014; Siddiqui et al., 2015; Wu et al., 2015). Here, at high concentrations of the two nano-CuO, similar developmental effects were observed (Supplementary Table S1), but the amounts of soluble copper measured after 96 h were different (50 ppb for 2000 ppb of synthesized nano-CuO and 31 ppb for 19 000 ppb of commercial nano-CuO), while at 50 ppb of CuSO_4 , milder developmental impacts were observed (Supplementary Table S1). This indicates that there is a nano-related effect with particulate copper causing more severe abnormal development than just based on the amount of soluble copper present.

In addition, the differences in toxicity might be due the amount of copper accumulated inside the embryos (Figure 6A). Embryos exposed to 1900 ppb and 19 000 ppb of commercial nano-CuO (where 16 ppb and 33 ppb of soluble copper was found in FSW, respectively) accumulated 1.2 and 2.2 times the amount of copper found in embryos exposed to 50 ppb of soluble copper. This indicates that soluble copper is not the only source of internalized copper, further supporting the observation that nano-CuO

Figure 5. Developmental effects on the skeleton of *Lytechinus pictus* embryos after 96 h of exposure to different sources of copper. (A) Normal development. (B) Underdeveloped skeleton. (C) Short postlarval arms. (D) Three elongated spicules. (E) Posterior view of an embryo with multiple triradiate spicules. (F) No spicule formation. Arrows indicate the areas where the gut is observed.

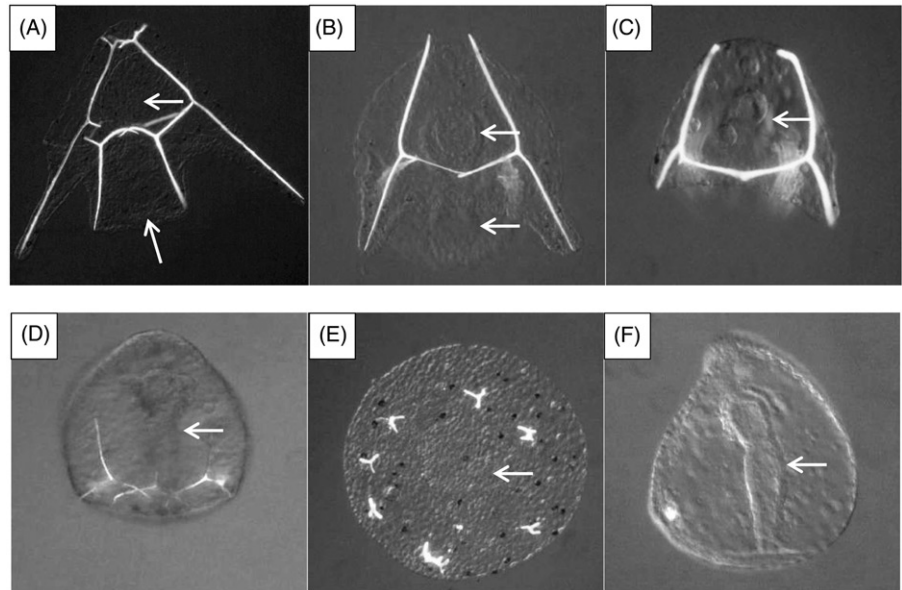
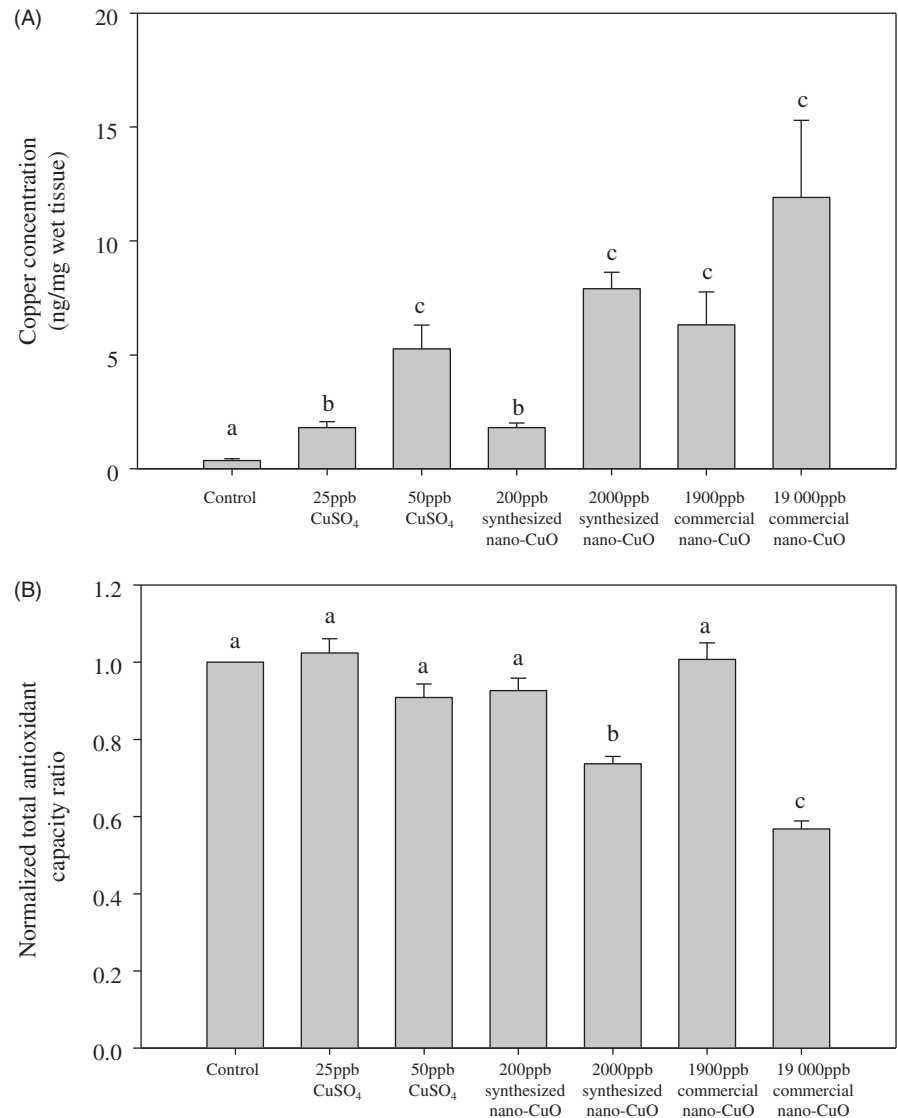


Figure 6. Internal copper concentrations and TAOC in sea urchin embryos exposed to copper sulfate and synthesized and commercial nano-CuO. (A) Tissue copper concentration. (B) TAOC in tissue homogenates; values were normalized to protein concentrations, and then compared with the control values. No direct correlation between copper accumulation and TAOC was observed, but the highest accumulation of copper occurred for 19 000 ppb of commercial nano-CuO where the lowest TAOC was observed. Different lower case letters represent statistical differences between treatments ($p < 0.05$).



aggregates are being internalized. As such, nano-CuO may follow the “Trojan horse”-type mechanism (Studer et al., 2010), delivering high concentrations of copper when aggregates dissolve inside the cell due to significantly lower cytoplasmic pH (Johnson & Epel, 1981), creating copper hot-spots, as has been demonstrated for other metal oxide NMs (Gilbert et al., 2012; Xia et al., 2008). Based on the differences in dissolution rates measured in FSW, it is reasonable to hypothesize that the NMs may have accentuated differences in dissolution rates inside the cells where pH is lower and there is higher protein concentration (Studer et al., 2010), resulting in higher solubility and toxicity of synthesized nano-CuO compared with commercial nano-CuO. A high intracellular concentration of Cu^{2+} can overwhelm the natural defenses against heavy metals, such as conjugation and effluxing through membrane transporters (Cole & Deeley, 2006). Commercial nano-CuO has been shown to increase the concentration of copper inside sea urchin embryos and inhibit the activity of ABC efflux transporters at low, non-toxic nano-CuO concentrations creating chemosensitization where other toxic chemicals become more toxic due to inhibition of efflux transport (Bosnjak et al., 2009; Wu et al., 2015). Furthermore, synthesized nano-CuO can chelate short chain protein and polypeptides, causing a decreased detoxification activity that can lead to a higher toxicity compared with commercial nano-CuO (Joshi et al., 2012).

Oxidative stress damage to proteins has been reported as an important toxic effect of NM exposure (Hu et al., 2014; Kovacic & Somanathan, 2010). In this study, no significant differences in protein oxidation were observed following copper exposure (Supplementary Figure S2). However, oxidative stress effects were observed for TAOC, which is a measure of the overall interactions and synergic effects of all the individual antioxidant mechanisms, both enzymatic as well as low-molecular weight antioxidants (Ghiselli et al., 2000). Significant differences in the TAOC were observed only at high concentrations of both nano-CuO (Figure 6B), indicating a “nano” effect occurred with respect to TAOC. Copper and copper oxide NMs are known to generate reactive oxygen species (ROS), altering the expression of antioxidant enzymes such as superoxide dismutase, catalase and glutathione peroxidase (Gomes et al., 2011; Hu et al., 2014; Triboulet et al., 2013; Wu et al., 2015). At high concentrations of nano-CuO, the concentration of ROS may exceed the antioxidant capacity. Furthermore, ROS can interact with the Cu^{2+} released during nano-CuO dissolution and cause inactivation of antioxidant enzymes through Fenton and Haber Weiss reactions (Gomes et al., 2011), while the excess Cu^{2+} can cause protein denaturation and degradation (Triboulet et al., 2013). It is possible that no significant changes in TAOC were observed for soluble copper because there was a balance between the expression of antioxidant enzymes and their inactivation, while the copper hot-spots generated by solubilized nano-CuO aggregates inside the embryos may have overwhelmed these defenses causing localized oxidative damage and decreased TAOC.

Regarding morphology, the most common developmental effects observed were malformation of the skeleton, delayed development, and bell-like shape embryos (Figures 4 and 5). The skeleton of sea urchin embryos consists of a number of calcite rods or spicules whose development is directed by the primary mesenchyme cells (PMCs) (Wolpert & Gustafson, 1961). Skeletogenesis begins when, on the ventral side of the embryo, PMCs form two triradiate spicules that later elongate following the specific pattern created by the PMCs, where calcium carbonate obtained from the surrounding environment is deposited (Guss & Etnensohn, 1997; Lyons et al., 2014; McIntyre et al., 2014; Okazaki, 1960). Cu^{2+} may decrease calcification by replacing Ca^{2+} , leading to larvae with shorter arms (Ghorani

et al., 2012), or an asymmetric skeleton (Byrne et al., 2013). In addition, copper can decrease the Ca^{2+} uptake by altering Ca-ATPase activity either by direct binding or by generating ROS that disrupts the cell membrane (Tellis et al., 2014). Other significant effects observed are related to altered axis determination. The sea urchin embryo is organized along two orthogonal axes of symmetry: the animal-vegetal axis (AV) and dorso-ventral axis (DV), also known as aboral-oral axis (AO) (Coffman & Davidson, 2001). While the AV axis is maternally determined in the egg (Horstadius, 1939), the AO axis is determined later during development in response to gene expression patterns generated by a redox gradient in the embryo (Coffman & Davidson, 2001). An abnormally high concentration of ROS can cause oralization of the ectoderm and alter the skeletal pattern created by the PMCs, producing supernumerary spicules, as occurs in embryos exposed to nickel (Coffman & Davidson, 2001; Hardin et al., 1992). Multiple spicules were observed in embryos exposed to copper (Figure 4D and E, Supplementary Figure S4B and D), meaning alterations of the ectoderm occurred probably due to an altered redox status induced by the copper hot-spots generated during nano-CuO dissolution. Another similarity with nickel treated embryos is the bell-like morphology (Figure 4G and H), also attributed to alterations of the AO axis (Hardin et al., 1992; Ryu et al., 2012). This suggests that copper and nickel might share similar mechanisms of disruption, probably related to altered gene expression and transcription, especially of genes related to AO axis determination (Agca et al., 2009; Hardin et al., 1992; Röttinger & Martindale, 2011; Ryu et al., 2012). Further analyses are necessary to demonstrate if copper alters the expression and transcription of the same or similar groups of genes.

The morphologies observed have important implications in survival. Delayed development and smaller size implies longer periods of time in the planktonic stage, increasing the probability of predation (Allen, 2008). The effects observed in skeleton development, whether it is decreased length, asymmetry or simply abnormal development (multiple spicules), all affect survival capabilities since normal arm skeletal rods are essential for feeding and swimming (Hart & Strathmann, 1994; Soars et al., 2009).

Nano-CuO has other toxic effects in aquatic organisms not related to development (Gomes et al., 2011; Hanna et al., 2014; Hanna et al., 2013; Hu et al., 2014; Lin et al., 2013). In zebrafish embryos, the soluble copper released from the nano-CuO inhibits the activity of the hatching enzyme in zebrafish embryos without affecting their morphology (Lin et al., 2013). In contrast, morphology of sea urchin embryos was impacted at comparatively lower concentrations with no effect on hatching for either nano-CuO or CuSO_4 (this study); this also has been observed in Pacific herring embryos in seawater (data not shown). This suggests that even though there is homology between the hatching enzymes in different aquatic embryos, differences in media (i.e. freshwater versus seawater) play an important role in metal ion toxicity (Kawaguchi et al., 2013; Nomura et al., 1997).

Conclusions

We have shown that the physicochemical characteristics of the nano-CuOs play an essential role in their toxicity, with both internalization and dissolution being the most important processes. Synthesized nano-CuO showed greater toxicity and had increased dissolution as compared with the less-pure commercial nano-CuO. This information may be useful to improve the design of nano-CuO-based antifouling paints, combining both chemical and physical strategies to prevent fouling of organisms, through a more localized dissolution and a modulated zeta potential, thus preventing the toxic effects on non-target organisms.

Copper causes specific developmental effects in sea urchin embryos by disrupting the aboral-oral axis which is probably related to altered gene expression induced by changes in the redox environment caused by dissolution of internalized CuO nanoparticles. Abnormal spicule formation is likely caused by both abnormal gene expression as well as altered calcification.

Declaration of interest

The authors report no conflicts of interest. The authors alone are responsible for the content and writing of the article. This research is part of the University of California Center for the Environmental Implications of Nanotechnology (UC CEIN) and was supported by the National Science Foundation and the Environmental Protection Agency under Cooperative Agreement Number DBI-0830117 and DBI-1266377. Any opinions, findings and conclusions or recommendations expressed in this material are those of the author(s) and do not necessarily reflect the views of the National Science Foundation or the Environmental Protection Agency. This work has not been subjected to EPA review and no official endorsement should be inferred. The authors would like to thank the funding from the UC MEXUS-CONAcYt Postdoctoral Research Fellowship program (C. Torres) and Carol Vines for technical support.

References

- Adeleye AS, Conway JR, Perez T, Rutten P, Keller AA. 2014. Influence of extracellular polymeric substances on the long-term fate, dissolution, and speciation of copper-based nanoparticles. *Environ Sci Technol* 48:12561–8.
- Adeleye AS, Keller AA. 2014. Long-term colloidal stability and metal leaching of single wall carbon nanotubes: effect of temperature and extracellular polymeric substances. *Water Res* 49:236–50.
- Adeleye AS, Keller AA, Miller RJ, Lenihan HS. 2013. Persistence of commercial nanoscaled zero-valent iron (nZVI) and by-products. *J Nanopart Res* 15:1–18.
- Agca C, Klein WH, Venuti JM. 2009. Respecification of ectoderm and altered Nodal expression in sea urchin embryos after cobalt and nickel treatment. *Mech Dev* 126:430–42.
- Allen JD. 2008. Size-specific predation on marine invertebrate larvae. *Biol Bull* 214:42–9.
- Amorim MJB, Scott-Fordsmand JJ. 2012. Toxicity of copper nanoparticles and CuCl₂ salt to *Enchytraeus albidus* worms: survival, reproduction and avoidance responses. *Environ Pollut* 164:164–8.
- Åsbrink S, Waškowska A. 1991. CuO: X-ray single-crystal structure determination at 196 K and room temperature. *J Phys Condens Matter* 3:8173–80.
- Bielmyer-Fraser GK, Jarvis TA, Lenihan HS, Miller RJ. 2014. Cellular partitioning of nanoparticulate versus dissolved metals in marine phytoplankton. *Environ Sci Technol* 48:13443–50.
- Bosnjak I, Uhlinger KR, Heim W, Smital T, Franekic-Colic J, Coale K, et al. 2009. Multidrug efflux transporters limit accumulation of inorganic, but not organic, mercury in sea urchin embryos. *Environ Sci Technol* 43:8374–80.
- Bradford MM. 1976. A rapid and sensitive method for the quantitation of microgram quantities of protein utilizing the principle of protein-dye binding. *Anal Biochem* 72:248–54.
- Byrne M, Lamare M, Winter D, Dworjanyan SA, Uthicke S. 2013. The stunting effect of a high CO₂ ocean on calcification and development in sea urchin larvae, a synthesis from the tropics to the poles. *Philos Trans R Soc Lond B Biol Sci* 368:20120439.
- Cao S, Wang J, Chen H, Chen D. 2011. Progress of marine biofouling and antifouling technologies. *Chin Sci Bull* 56:598–612.
- Coffman JA, Davidson EH. 2001. Oral-aboral axis specification in the sea urchin embryo. I. Axis entrainment by respiratory asymmetry. *Dev Biol* 230:18–28.
- Cole SPC, Deeley RG. 2006. Transport of glutathione and glutathione conjugates by MRP1. *Trends Pharmacol Sci* 27:438–46.
- Conway JR, Adeleye AS, Gardea-Torresdey J, Keller AA. 2015. Aggregation, dissolution, and transformation of copper nanoparticles in natural waters. *Environ Sci Technol* 49:2749–56.
- Covian-Nares JF, Smith RM, Vogel SS. 2008. Two independent forms of endocytosis maintain embryonic cell surface homeostasis during early development. *Dev Biol* 316:135–48.
- Cho W-S, Duffin R, Thielbeer F, Bradley M, Megson IL, MacNee W, et al. 2012. Zeta potential and solubility to toxic ions as mechanisms of lung inflammation caused by metal/metal oxide nanoparticles. *Toxicol Sci* 126:469–77.
- Durand A, Chase Z, Remenyi T, Quéroué F. 2013. Microplate-reader method for the rapid analysis of copper in natural waters with chemiluminescence detection. *Front Microbiol* 3:437.
- Fairbairn EA, Keller AA, Mädler L, Zhou D, Pokhrel S, Cherr GN. 2011. Metal oxide nanomaterials in seawater: linking physicochemical characteristics with biological response in sea urchin development. *J Hazard Mat* 192:1565–71.
- Fernández N, Beiras R. 2001. Combined toxicity of dissolved mercury with copper, lead and cadmium on embryogenesis and early larval growth of the *Paracentrotus lividus* sea-urchin. *Ecotoxicology* 10: 263–71.
- Garner KL, Suh S, Lenihan HS, Keller AA. 2015. Species sensitivity distributions for engineered nanomaterials. *Environ Sci Technol* 49: 5753–9.
- George S, Lin S, Ji Z, Thomas CR, Li L, Mecklenburg M, et al. 2012. Surface defects on plate-shaped silver nanoparticles contribute to its hazard potential in a fish gill cell line and zebrafish embryos. *ACS Nano* 6:3745–59.
- George S, Xia T, Rallo R, Zhao Y, Ji Z, Lin S, et al. 2011. Use of a high-throughput screening approach coupled with in vivo zebrafish embryo screening to develop hazard ranking for engineered nanomaterials. *ACS Nano* 5:1805–17.
- Ghiselli A, Serafini M, Natella F, Scaccini C. 2000. Total antioxidant capacity as a tool to assess redox status: critical view and experimental data. *Free Radic Biol Med* 29:1106–14.
- Ghorani V, Mahdavi Shahri N, Ghassemzadeh Z, Mortazavi MS, Mohammadi E, Sadripour E. 2012. The effect of lead toxicity on embryonic development and early larval growth of the *Echinometra mathaei* sea urchin (Persian Gulf), morphologic and morphometric studies. *Ann Biol Res* 3:3321–7.
- Gilbert B, Fakra SC, Xia T, Pokhrel S, Mädler L, Nel A. 2012. The fate of ZnO nanoparticles administered to human bronchial epithelial cells. *ACS Nano* 6:4921–30.
- Gomes T, Pinheiro JP, Cancio I, Pereira CG, Cardoso C, Bebianno MJ. 2011. Effects of copper nanoparticles exposure in the mussel *Mytilus galloprovincialis*. *Environ Sci Technol* 45:9356–62.
- Gunawan C, Teoh WY, Marquis CP, Amal R. 2011. Cytotoxic origin of copper(II) oxide nanoparticles: comparative studies with micron-sized particles, leachate, and metal salts. *ACS Nano* 5:7214–25.
- Guss KA, Etensohn CA. 1997. Skeletal morphogenesis in the sea urchin embryo: regulation of primary mesenchyme gene expression and skeletal rod growth by ectoderm-derived cues. *Development* 124: 1899–908.
- Hamdoun A, Epel D. 2007. Embryo stability and vulnerability in an always changing world. *Proc Natl Acad Sci USA* 104:1745–50.
- Hanna S, Miller R, Lenihan H. 2014. Accumulation and toxicity of copper oxide engineered nanoparticles in a marine mussel. *Nanomaterials* 4:535–47.
- Hanna SK, Miller RJ, Zhou D, Keller AA, Lenihan HS. 2013. Accumulation and toxicity of metal oxide nanoparticles in a soft-sediment estuarine amphipod. *Aquat Toxicol* 142–3:441–6.
- Hardin J, Coffman JA, Black SD, McClay DR. 1992. Commitment along the dorsoventral axis of the sea urchin embryo is altered in response to NiCl₂. *Development* 116:671–85.
- Hart MW, Strathmann RR. 1994. Functional consequences of phenotypic plasticity in echinoid larvae. *Biol Bull* 186:291–9.
- Horstadius S. 1939. The mechanics of sea urchin development, studied by operative methods. *Biol Rev* 14:132–79.
- Hu W, Culloty S, Darmody G, Lynch S, Davenport J, Ramirez-Garcia S, et al. 2014. Toxicity of copper oxide nanoparticles in the blue mussel, *Mytilus edulis*: a redox proteomic investigation. *Chemosphere* 108: 289–99.
- Johnson CH, Epel D. 1981. Intracellular pH of sea urchin eggs measured by the dimethylloxalidinedione (DMO) method. *J Cell Biol* 89: 284–91.
- Joshi S, Ghosh I, Pokhrel S, Mädler L, Nau WM. 2012. Interactions of amino acids and polypeptides with metal oxide nanoparticles probed by fluorescent indicator adsorption and displacement. *ACS Nano* 6: 5668–79.
- Kawaguchi M, Yasumasu S, Shimizu A, Kudo N, Sano K, Iuchi I, Nishida M. 2013. Adaptive evolution of fish hatching enzyme: one amino acid

- substitution results in differential salt dependency of the enzyme. *J Exp Biol* 216:1609–15.
- Keller AA, Wang H, Zhou D, Lenihan HS, Cherr G, Cardinale BJ, et al. 2010. Stability and aggregation of metal oxide nanoparticles in natural aqueous matrices. *Environ Sci Technol* 44:1962–7.
- King CK, Riddle MJ. 2001. Effects of metal contaminants on the development of the common Antarctic sea urchin *Sterechninus neumayeri* and comparisons of sensitivity with tropical and temperate echinoids. *Mar Ecol Prog Ser* 215:143–54.
- Kobayashi N, Okamura H. 2004. Effects of heavy metals on sea urchin embryo development. 1. Tracing the cause by the effects. *Chemosphere* 55:1403–12.
- Kovacic P, Somanathan R. 2010. Biomechanisms of nanoparticles (toxicants, antioxidants and therapeutics): electron transfer and reactive oxygen species. *J Nanosci Nanotechnol* 10:7919–30.
- Lin S, Zhao Y, Ji Z, Ear J, Chang CH, Zhang H, et al. 2013. Zebrafish high-throughput screening to study the impact of dissolvable metal oxide nanoparticles on the hatching enzyme, ZHE1. *Small* 9:1776–85.
- Lin S, Zhao Y, Xia T, Meng H, Ji Z, Liu R, et al. 2011. High content screening in zebrafish speeds up hazard ranking of transition metal oxide nanoparticles. *ACS Nano* 5:7284–95.
- Loosli F, Le Coustumer P, Stoll S. 2013. TiO₂ nanoparticles aggregation and disaggregation in presence of alginate and Suwannee River humic acids. pH and concentration effects on nanoparticle stability. *Water Res* 47:6052–63.
- Lyons DC, Martik ML, Saunders LR, McClay DR. 2014. Specification to biomineralization: following a single cell type as it constructs a skeleton. *Integr Comp Biol* 54:723–33.
- McIntyre DC, Lyons DC, Martik M, McClay DR. 2014. Branching out: origins of the sea urchin larval skeleton in development and evolution. *Genesis* 52:173–85.
- Midander K, Cronholm P, Karlsson HL, Elihn K, Möller L, Leygraf C, Wallinder IO. 2009. Surface characteristics, copper release, and toxicity of nano- and micrometer-sized copper and copper(II) oxide particles: a cross-disciplinary study. *Small* 5:389–99.
- Miller NJ, Rice-Evans C. 1997. Factors influencing the antioxidant activity determined by the ABTS⁺ radical cation assay. *Free Radic Res* 26:195–9.
- Nel AE, Mädler L, Velegol D, Xia T, Hoek EMV, Somasundaran P, et al. 2009. Understanding biophysicochemical interactions at the nano-bio interface. *Nat Mater* 8:543–57.
- Nomura K, Shimizu T, Kinoh H, Sendai Y, Inomata M, Suzuki N. 1997. Sea urchin hatching enzyme (Envelysin): cDNA cloning and deprivation of protein substrate specificity by autolytic degradation. *Biochemistry* 36:7225–38.
- Oberdorster G. 2010. Safety assessment for nanotechnology and nanomedicine: concepts of nanotoxicology. *J Int Med* 267:89–105.
- Okazaki K. 1960. Skeleton formation of sea urchin larvae. *Embryologia* 5:283–320.
- Pillai MC, Vines CA, Wikramanayake AH, Cherr GN. 2003. Polycyclic aromatic hydrocarbons disrupt axial development in sea urchin embryos through a b-catenin dependent pathway. *Toxicology* 186:93–108.
- Pokhrel S, Birkenstock J, Schowalter M, Rosenauer A, Mädler L. 2009. Growth of ultrafine single crystalline WO₃ nanoparticles using flame spray pyrolysis. *Cryst Growth Des* 10:632–9.
- Pokhrel S, Nel AE, Mädler L. 2012. Custom-designed nanomaterial libraries for testing metal oxide toxicity. *Acc Chem Res* 46:632–41.
- Rawat J, Ray S, Rao P, Choudary NV. 2010. Recent developments of nanomaterial doped paints for the minimization of biofouling in submerged structures. *Mater Sci Forum* 657:75–82.
- Rosen G, Rivera-Duarte I, Bart Chadwick D, Ryan A, Santore RC, Paquin PR. 2008. Critical tissue copper residues for marine bivalve (*Mytilus galloprovincialis*) and echinoderm (*Strongylocentrotus purpuratus*) embryonic development: conceptual, regulatory and environmental implications. *Mar Environ Res* 66:327–36.
- Röttinger E, Martindale MQ. 2011. Ventralization of an indirect developing hemichordate by NiCl₂ suggests a conserved mechanism of dorso-ventral (D/V) patterning in *Ambulacraria* (hemichordates and echinoderms). *Dev Biol* 354:173–90.
- Ryu TK, Lee G, Rhee Y, Park H-S, Chang M, Lee S, et al. 2012. Identification of nickel response genes in abnormal early developments of sea urchin by differential display polymerase chain reaction. *Ecotoxicol Environ Saf* 84:18–24.
- Shacter E. 2000. Quantification and significance of protein oxidation in biological samples. *Drug Metab Rev* 32:307–26.
- Shi J, Abid AD, Kennedy IM, Hristova KR, Silk WK. 2011. To duckweeds (*Landoltia punctata*), nanoparticulate copper oxide is more inhibitory than the soluble copper in the bulk solution. *Environ Pollut* 159:1277–82.
- Siddiqui S, Goddard RH, Bielmyer-Fraser GK. 2015. Comparative effects of dissolved copper and copper oxide nanoparticle exposure to the sea anemone, *Exaiptasia pallida*. *Aquat Toxicol* 160:205–13.
- Soars N, Prowse T, Byrne M. 2009. Overview of phenotypic plasticity in echinoid larvae, '*Echinopluteus transversus*' type vs. typical echinoplutei. *Mar Ecol Prog Ser* 383:113–25.
- Studer AM, Limbach LK, Van Duc L, Krumeich F, Athanassiou EK, Gerber LC, et al. 2010. Nanoparticle cytotoxicity depends on intracellular solubility: comparison of stabilized copper metal and degradable copper oxide nanoparticles. *Toxicol Lett* 197:169–74.
- Tellis M, Lauer M, Nadella S, Bianchini A, Wood C. 2014. The effects of copper and nickel on the embryonic life stages of the purple sea urchin (*Strongylocentrotus purpuratus*). *Arch Environ Contam Toxicol* 67:453–64.
- Teoh WY, Amal R, Mädler L. 2010. Flame spray pyrolysis: an enabling technology for nanoparticles design and fabrication. *Nanoscale* 2:1324–47.
- Thit A, Selck H, Bjerregaard HF. 2013. Toxicity of CuO nanoparticles and Cu ions to tight epithelial cells from *Xenopus laevis* (A6): effects on proliferation, cell cycle progression and cell death. *Toxicol In Vitro* 27:1596–601.
- Triboulet S, Aude-Garcia C, Carrière M, Diemer H, Proamer F, Habert A, et al. 2013. Molecular responses of mouse macrophages to copper and copper oxide nanoparticles inferred from proteomic analyses. *Mol Cell Proteomics* 12:3108–22.
- Wolpert L, Gustafson T. 1961. Studies on the cellular basis of morphogenesis of the sea urchin embryo. Development of the skeletal pattern. *Exp Cell Res* 25:311–25.
- Wu B, Torres-Duarte C, Cole B, Cherr GN. 2015. Copper oxide and zinc oxide nanomaterials act as inhibitors of multidrug resistance transport in sea urchin embryos: their role as chemosensitizers. *Environ Sci Technol* 49:5760–70.
- Xia T, Kovochich M, Liong M, Mädler L, Gilbert B, Shi H, et al. 2008. Comparison of the mechanism of toxicity of zinc oxide and cerium oxide nanoparticles based on dissolution and oxidative stress properties. *ACS Nano* 2:2121–34.
- Xia T, Zhao Y, Sager T, George S, Pokhrel S, Li N, et al. 2011. Decreased dissolution of ZnO by iron doping yields nanoparticles with reduced toxicity in the rodent lung and zebrafish embryos. *ACS Nano* 5:1223–35.
- Zhang H, Ji Z, Xia T, Meng H, Low-Kam C, Liu R, et al. 2012. Use of metal oxide nanoparticle band gap to develop a predictive paradigm for oxidative stress and acute pulmonary inflammation. *ACS Nano* 6:4349–68.

Supplementary material available online.
 Figures S1–S5 and Tables S1 and S2.